

Simulations of wind turbine rotor with vortex generators

Niels Troldborg, Frederik Zahle, Niels N. Sørensen

DTU Wind Energy, Technical University of Denmark, Risø Campus, Denmark

E-mail: niet@dtu.dk

Abstract. This work presents simulations of the DTU 10MW wind turbine rotor equipped with vortex generators (VGs) on the inner part of the blades. The objective is to study the influence of different VG configurations on rotor performance and in particular to investigate the radial dependence of VGs, i.e. how VGs at one section of the blade may affect the aerodynamic characteristics at other radial positions. Furthermore, the performance of different sections on the blade is compared to their corresponding performance in 2D flow.

1. Introduction

A vortex generator (VG) is a small vane which is typically attached to the suction side of wings/blades, where it causes local mixing in the boundary layer and thereby can delay/prevent flow separation [22]. Therefore, VGs can enhance the aerodynamic performance of blades/wings at high angles of attack which is also why VGs today are widely used for passive flow control.[10, 9, 21, 20, 25]

The engineering design codes used by wind energy industry today typically take into account the effect of VGs by using modified aerofoil characteristics. These data are usually obtained through wind tunnel experiments [5]. However, such measurements are costly and can be difficult to perform at sufficiently high Reynolds numbers as well as on the relatively thick aerofoil sections which are normally used on wind turbine blades today. Furthermore, measurements on aerofoil sections in 2D does not take into account possible 3D effects and radial dependence which are known to exist on wind turbine blades. Alternatively, one can use CFD to compute the effect of the VGs. Sørensen et al. [19] presented RANS simulations of a 30% and 36% thick aerofoil section, equipped with a VG, in which the VG was resolved with a grid. The simulated lift on the thin aerofoil was generally in good agreement with measurements but when the VG was placed aft on the aerofoil the lift was generally somewhat underestimated. For the thick aerofoil the simulations generally overestimated maximum lift. For both aerofoils the computations underestimated drag. The reason for the deviation are partly due to the well known limitations of RANS turbulence and transition models and partly because the VGs in the measurements were mounted on the aerofoil via a baseplate, which was not included in the simulations. Despite the differences, their work showed that CFD is capable of predicting the qualitative effect of VGs and can be used to compare different VG setups. However, due to the large range of scales present for a wing equipped with VGs, it is not computationally feasible to directly simulate a full wind turbine blade equipped with many VGs. To overcome this difficulty Bender et al. [3] developed the so-called BAY model in which the VGs are modelled by adding body forces in the



momentum equations and thereby removing the need of a mesh around the individual VG. This model has been validated and calibrated against both measurements and fully gridded CFD for a variety of flow cases [9, 1, 3, 4, 7]. These studies have proven that the BAY model is capable of capturing the effect of VGs with far fewer grid points than fully resolved CFD.

In this work we present simulations of a wind turbine rotor with and without a row of VGs on the blades and compare the results to corresponding simulations on extruded aerofoil sections. In the simulations the wind turbine rotor and aerofoils are fully resolved by a grid, while the VGs are modelled using a modified version of the BAY model. The objective is to compare extruded 2D and 3D aerofoil characteristics and study how these are affected by the presence of VGs.

2. Methods

The model used for simulating the VGs is based on the BAY model [3], in which the VGs are represented as body forces which are determined by the VG shape and the local flow conditions using an analogy to thin aerofoil theory. Unlike the original BAY model, the model used in this work [24] more accurately represents the actual shape of the VGs, by modelling them as infinitely thin triangular actuator disks. All simulations are carried out using the incompressible Reynolds Averaged Navier-Stokes (RANS) solver EllipSys3D [12, 13, 16]. This code solves the incompressible finite volume Reynolds-Averaged Navier-Stokes (RANS) equations in general curvilinear coordinates in a collocated grid arrangement to facilitate complex mesh geometries. The VG body forces are applied into the computational domain by using the actuator shape model [15] and a modified Rhie-Chow algorithm [14, 23] to avoid odd/even pressure decoupling. In order to compare 2D and 3D aerofoil characteristics of aerofoils with and without VGs, simulations were carried out on both a full wind turbine rotor and on selected aerofoils with the same cross sections as on the wind turbine rotor.

2.1. Rotor simulations

The DTU 10 MW wind turbine [2] with and without a row of VGs fitted on the inboard part of the blades was used as a basis for the 3D rotor simulations. This turbine is an open source research turbine, including fully documented geometry, aero elastic and structural models as well as 3D CFD rotor meshes. The rotor has a radius of 89.166 m and uses the publicly available FFA-W3 aerofoil series along the entire blade.

Two different VG configurations are considered in the present work: C1) The leading edge of the VGs are positioned along a line starting at a chord-wise position of $0.5c$ at a span-wise position of $r=5$ m ($r/R=0.06$) and ends at approximately $0.21c$ at $r=30$ m ($r/R=0.3$), where c denotes the local chord length and R the rotor radius. C2) As in C1 but where the leading edge of the VGs are all at $0.21c$.

In both configurations the VG set-up is as shown in Figure 1, where $\beta = \pm 16^\circ$, $h = 0.01c_{max}$, $l = 0.04c_{max}$, $\Delta 1 = 0.045c_{max}$ and $\Delta 2 = 0.055c_{max}$, where $c_{max} = 6.2$ m is the max chord of the blade.

The spacing, angles and size of the VGs used in the two configurations are chosen rather arbitrarily but are representative for a standard VG setup. The positioning along the chord is also somewhat arbitrary but allows for a fundamental study of the radial dependence VGs may have on each other.

Figure 2 compares the chord-wise position of the leading edge of the VGs with the corresponding position of maximum thickness.

The simulations used the steady state moving mesh option in EllipSys3D [18] and assumed a fully developed turbulent boundary layer on the blade surface using the $k-\omega$ SST [11] turbulence model.

The use of steady state RANS is of course questionable for representing the highly separated

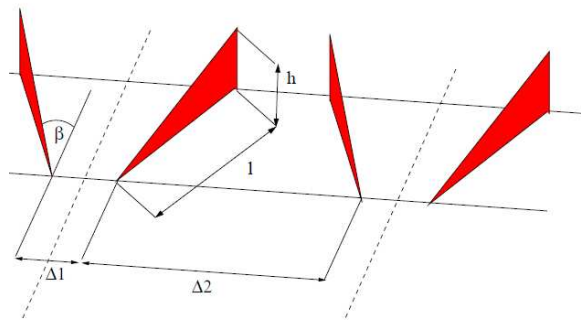


Figure 1. Sketch defining the dimensions of the used VG setup

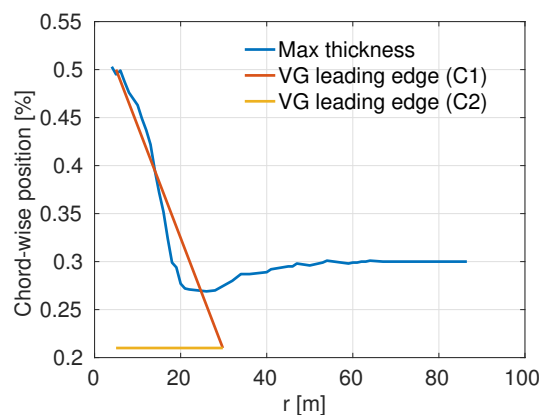


Figure 2. Comparison of chord-wise position of maximum thickness and VG leading edge.

and unsteady flows on the inboard part of the blades, however, it is a necessary simplification to keep the computational costs at a reasonable level. A risk of using steady state simulations to represent flow regions which are unsteady and/or oscillates between multiple states, and therefore will not converge, is that only one state is captured. This issue is partly addressed by averaging the aerofoil data over the last 3000 iterations of the simulations. It should be emphasized that even unsteady RANS and DES are also questionable for representing the flow at high angles of attack due to limitations in boundary layer turbulence and transition modelling. The computational mesh is the same as used in previous work [24]. The surface mesh was generated using the Python based in-house developed Parametric Geometry Library (PGL) tool. PGL uses simple parametric inputs about the blade, i.e. twist, chord and thickness distributions as well as aerofoil series, to automatically generate the surface mesh including the root and tip regions. The rotor surface mesh consisted of 256 cells in the chord-wise direction and 480 cells in the span-wise direction with a 64×64 cells tip cap on each blade tip. In the region of the blades where VGs are installed the cell length in the span-wise direction is 0.0775 m , corresponding to 8 cells per VG pair in agreement with the requirements found in previous work [24]. The volume mesh was of the O-O type and was generated using the hyperbolic mesh generator HypGrid [17]. To obtain a y^+ of less than 2 the height of the first cell in the boundary layer is set to $2 \times 10^{-6} \text{ m}$. The volume mesh is grown away from the surface using 128 cells in the normal direction to form a sphere with a radius of approximately 20 rotor radii.

2.2. Aerofoil simulations

Extruded 2D simulations were carried out on aerofoils with the same cross-sectional shape as on selected sections of the DTU 10 MW wind turbine. The simulations were conducted in steady state using the same turbulence model as the rotor simulations and at the same Reynolds number so that a one-to-one comparison could be made of their performance with and without 3D rotational effects.

The grids used for the aerofoil simulations were of the O-mesh type. The domain height and span-wise extent was set to approximately 30 and 0.4 chord lengths, respectively. The grid resolution was the same as used in the rotor simulations, i.e. 256, 128 and 32 cells in the chord-wise, normal and span-wise direction. Note that the used span-wise resolution corresponds to 8 cells per VG pair and thus that 4 VG pairs were modelled in these simulations.

3. Results

Figure 4 visualizes the flow over the inner part of the blade both with and without VGs at a free-stream velocity of 10 m/s, where the turbine operates with a rotational speed of 0.841 rad/s and a pitch of 0° .

When there are no VGs the flow clearly separates and shortly after begins to flow radially outwards due to the centrifugal force. When VGs are present they induce counter rotating vortices which add momentum to the boundary layer. In C1 these vortices effectively prevent flow separation for $r > 21$ m causing the flow to be rather 2D in that region. Further inboard the VGs in C1 cannot prevent separation but seems to slightly delaying it. The inner most VGs in C1 are on the other hand located downstream of the separation line for the clean blade and therefore are ineffective in preventing stall. In C2 the VGs delays separation in the region from 9 m $< r < 12$ m however, the price paid are regions further outboard (12 m $< r < 16$ m and 22 m $< r < 25$ m) with highly separated flow which are not seen in C1.

Figure 3 compares the tangential and normal force distribution in the three cases. As expected the VGs in C1 increase performance from 21 m $< r < 30$ m compare to the clean case. The distributions in C2 are characterized by significant dips at the radial positions where the flow stalls. These dips causes the rotor to perform worse with VGs in C2 than in the clean case. Figure 5 and 6 show the lift and drag curves of the blade sections at $r = 24$ m and $r = 28$ m,

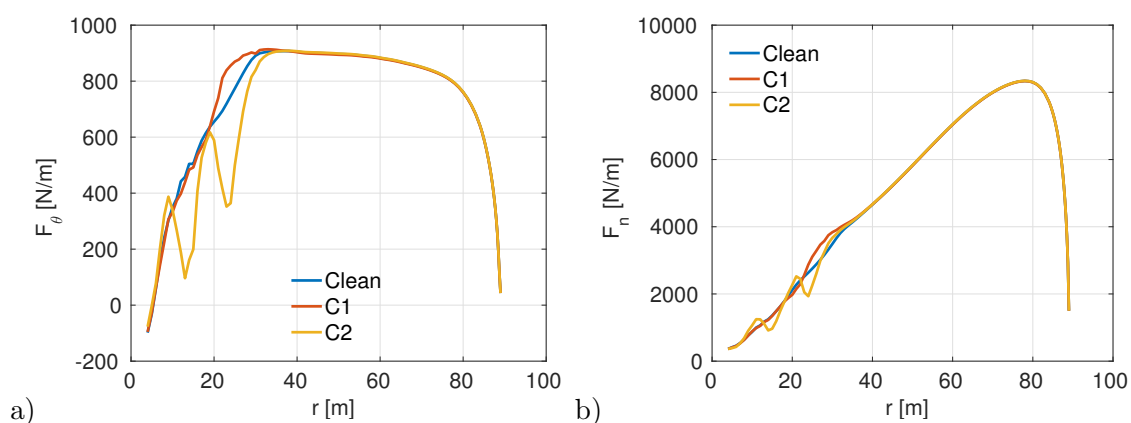


Figure 3. Tangential (a) and normal (b) force distribution in the three cases.

respectively both with and without VGs. The 3D aerofoil data was computed using the azimuthal averaging technique (AAT) [6, 8].

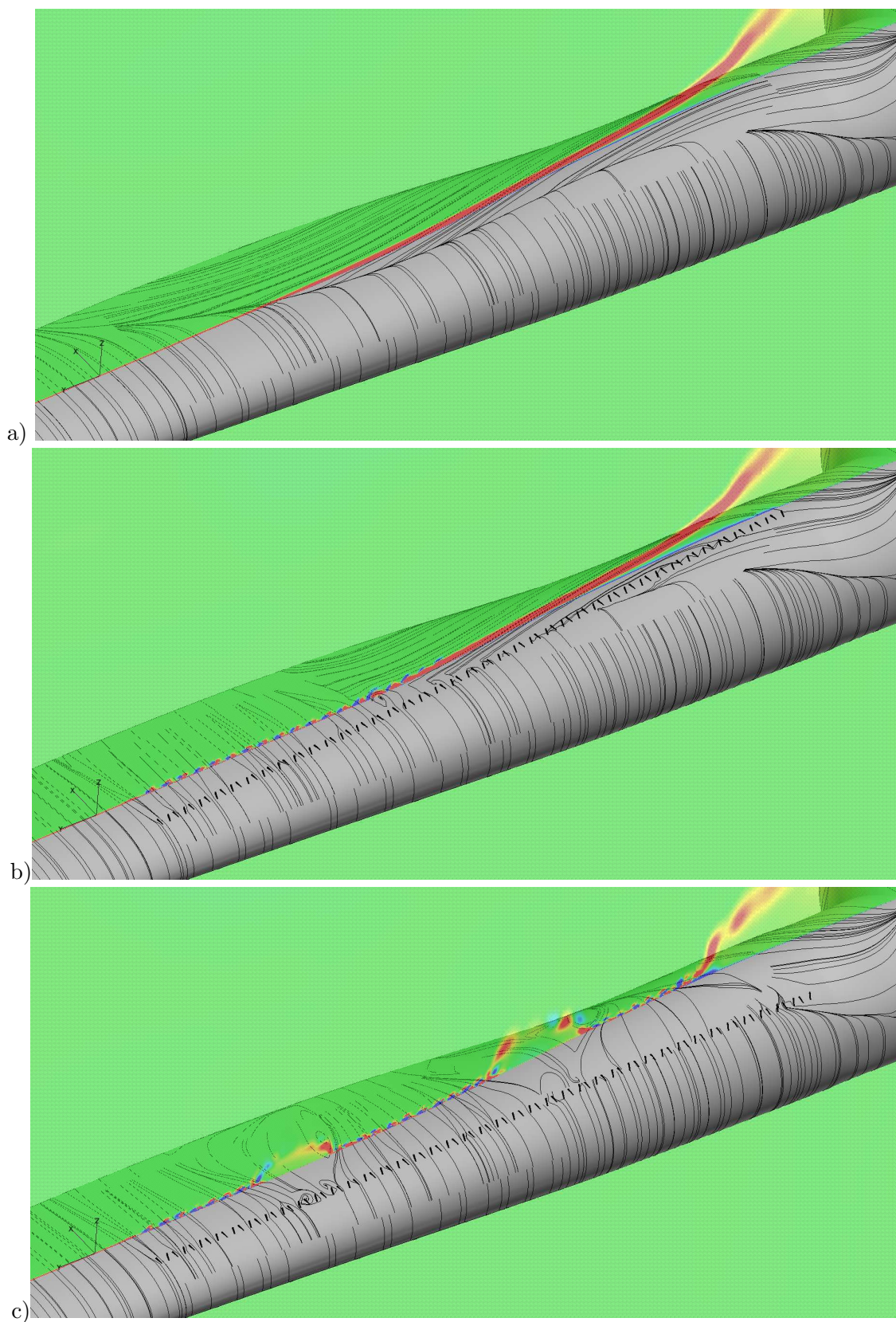


Figure 4. Surface restricted streamlines and tangential vorticity at the inboard part of the blade at a free-stream velocity of $V_0 = 10$ m/s. a) no VGs; b) VG config. 1; c) VG config. 2

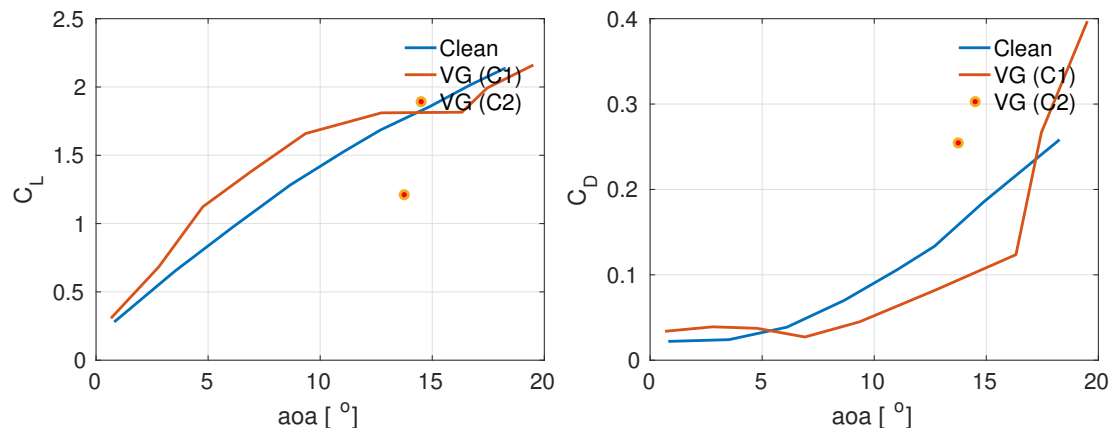


Figure 5. Lift and drag curves for the aerofoil section at $r = 24$ m

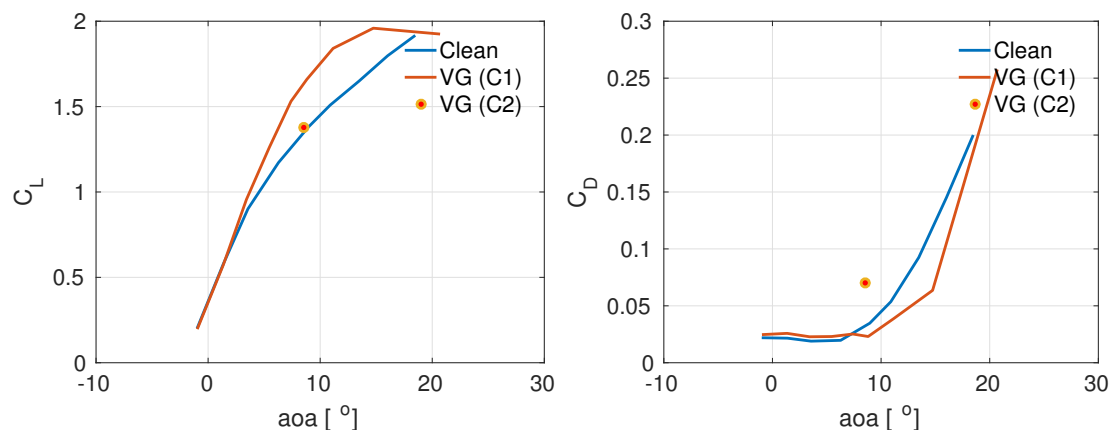


Figure 6. Lift and drag curves for the aerofoil section at $r = 28$ m

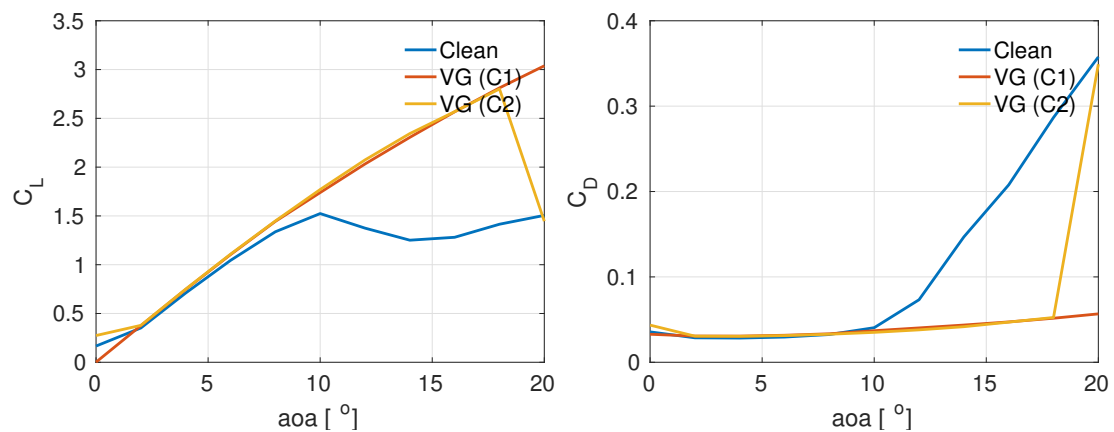


Figure 7. Extruded 2D predictions of lift and drag curves for the aerofoil section at $r = 24$ m

In order to get different angles of attack (aoa), while keeping the local Reynolds number unchanged, the aerofoil data was computed with the rotor operating at 10 m/s at the same rotational speed of 0.841 rad/s and then vary the pitch setting. Note that only one simulation is carried out on the rotor with VG configuration C2 and therefore there is only one point on the polars in this case. As expected the aerofoil sections with VG configuration C2 performs poorer than both C1 and the clean case. Since the chord-wise positions of the VGs at these spanwise positions are close to each other in C1 and C2 the differences in performance is expected to be due to effects occurring at other radial stations. The rather high lift levels reached in the clean case are mainly due to 3D effects: As seen in Figure 4 there is still a significant flow outwards at these sections. Due to the Coriolis force this radial flow induces a favourable pressure gradient which again increases the stream-wise momentum in the boundary layer and hence delays stall. In order to verify that the differences in performance are not due to the small differences in chord-wise position of the VGs, we performed extruded 2D aerofoil computations on the aerofoil section at $r = 24\text{ m}$ where the VGs were positioned exactly as in the two rotor cases, i.e. VG chord position of $x/c = 0.28$ and $x/c = 0.21$. The predicted results are shown in Figure 7.

As seen the aerofoil performance of this aerofoil section is nearly the same for the two VG positions and therefore shows that the dramatic change in performance of this section on the rotor is due to 3D rotational effects and radial dependence of the VGs. Comparing Figure 7 to Figure 5 it is seen that the lift of the aerofoil with VGs in the extruded 2D cases reaches much higher values than in 3D. The reason for this is not fully understood and requires more studies. Figure 8 compares the 2D and 3D aerofoil data for the section at $r = 28\text{ m}$ with and without VGs. Note that the VGs are in their C1 configuration.

The effect of the VG is (both in 2D and 3D) to increase lift and decrease drag at high angles of attack. At high angles of attack the rotational effect, as expected, enhances lift markedly above the corresponding 2D flow cases. However, when VGs are present the 3D lift curve flattens out at an angle of attack around 15 degree, whereas the lift slope for the aerofoil without VGs remains high here. The radial flow in the clean case enhances lift by virtue of the Coriolis force. On the other hand VGs increase chord-wise momentum and delays separation, which in effect reduce the radial flow and thus the beneficial Coriolis effect. Explaining the interplay between the VGs and Coriolis effect is complicated and requires further investigations. As seen, another effect of the rotational effects is to shift the lift curves to the left at low angles of attack and that this shift apparently is rather independent of the presence of the VGs.

4. Conclusions

Simulations of a wind turbine rotor equipped with a row of VGs on the blades have been carried out and the results are compared to corresponding simulations in extruded 2D flow. The results shows that the performance of a blade section on the rotor with VGs is affected by the presence of VGs on other sections. This suggest that accounting for the effect of VGs in aero-elastic codes by using modified aerofoil characteristics obtained from wind tunnel measurements or extruded 2D simulations may be problematic because these methods assumes radial independence of the blade sections.

Furthermore, it is shown that the presence of the VGs on the rotor may reduce the lift enhancement due to rotational effect at high angles of attack but seemingly does not affect the 3D effects at low angles of attack.

References

- [1] B.G. Allan, C.S. Yao, and J.C Lin. Numerical Simulation of Vortex Generator Vanes and Jets on a Flat Plate. *AIAA*, 2002-3160, 2002.
- [2] C. Bak, F. Zahle, R. Bitsche, T. Kim, A. Yde, L.C. Henriksen, P.B. Andersen, A. Natarajan, and M.H. Hansen. Design and performance of a 10 MW wind turbine. *To be submitted for Wind Energy*, 2014.

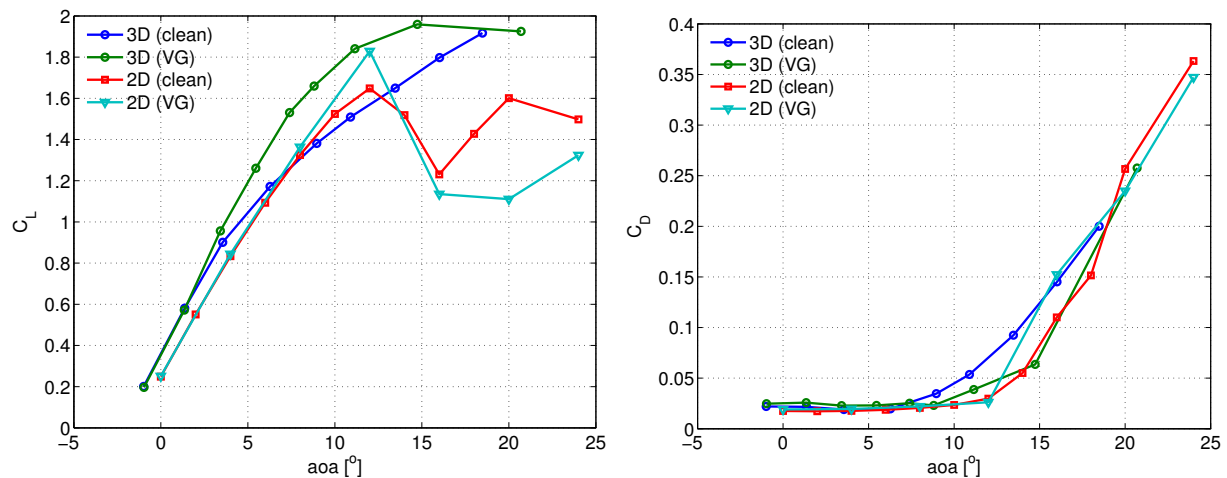


Figure 8. 2D/3D lift and drag curves for the aerofoil section at $r = 28$ m with and without VGs. The VGs are located in C1 configuration.

- [3] E.E. Bender, B.H. Anderson, and P.J. Yagles. Vortex generator modeling for Navier-Stokes codes. *Proceedings of the 1999 3rd ASME/JSME Joint Fluids Engineering Conference, San Francisco, California, USA, FEDSM99-6919*, 1999.
- [4] E.E. Bender, P.J. Yagles, D.N. Miller, and P.P. Traux. A Study of MEMS Flow Control for the Management of Engine Distortion in Compact Inlet Systems. *Proceedings of the 1999 3rd ASME/JSME Joint Fluids Engineering Conference, San Francisco, California, USA, FEDSM99-6920*, 1999.
- [5] G. Godard and M. Stanislas. Control of a decelerating boundary layer. *Aerospace Science and Technology*, 2006.
- [6] M.O.L. Hansen and J. Johansen. Tip studies using CFD and computation with tip loss models. *Wind Energy*, 7, 2004.
- [7] A. Jirasék. A Vortex Generator Model and its Application to Flow Control. *Proceedings of the 22nd Applied Aerodynamics Conference and Exhibit, Providence, Rhode Island, AIAA 2004-4965*, 2004.
- [8] J. Johansen and N.N. Sørensen. Airfoil characteristics from 3D CFD rotor computations. *Wind Energy*, 7, 2004.
- [9] J.C. Lin. Review of research on low-profile vortex generators to control boundary layer separation. *Progress in Aerospace Sciences*, 38:389–420, 2002.
- [10] J.C. Lin, S.K. Robinson, R.J. McGhee, and W.O. Valerezo. Separation Control on High-Lift Airfoils via Micro-Vortex Generators. *Journal of Aircraft*, 31:1317–1323, 1994.
- [11] F.R. Menter. Zonal Two Equation $k-\omega$ Turbulence Models for Aerodynamic Flows. *AIAA Journal*, (93-2906), 1993.
- [12] J.A. Michelsen. Basis3D - a platform for development of multiblock PDE solvers. Technical report AFM 92-05, Technical University of Denmark, Lyngby, 1992.
- [13] J.A. Michelsen. Block structured multigrid solution of 2D and 3D elliptic PDEs. Technical Report AFM 94-06, Technical University of Denmark, 1994.
- [14] P.-E. Réthoré and N. N. Sørensen. A discrete force allocation algorithm for modelling wind turbines in computational fluid dynamics. *Wind Energy*, 15:915–926, 2012.
- [15] P.-E. Réthoré, P. van der Laan, N. Troldborg, F. Zahle, and N. N. Sørensen. Verification and validation of an actuator disc model. *Wind Energy*, 17:919–937, 2013.
- [16] N.N. Sørensen. *General Purpose Flow Solver Applied to Flow over Hills*. PhD thesis, Technical University of Denmark, 1995.
- [17] N.N. Sørensen. HyGrid a 2-D Mesh Generator. Technical report, Risø National Laboratory, 1998.
- [18] N.N. Sørensen. Rotor computations using a 'steady state' moving mesh. *IEA Joint Action Committee on aerodynamics. Annex XI and 20. Aero experts meeting, Pamplona (ES), 25-26 May*, 2005.
- [19] N.N. Sørensen, F. Zahle, C. Bak, and T. Vronsky. Prediction of the Effect of Vortex Generators on Airfoil Performance. *Torque conference 2014, Lyngby, Denmark*, 2014.
- [20] T.L. Sullivan. Effect of vortex generators on the power conversion performance and structural dynamic loads

- of the MOD-2 wind turbine. Technical report, NASA, 1984.
- [21] T. Tai. Effect of micro-vortex generators on V-22 aircraft forward-flight aerodynamics. *40th AIAA Aerospace Sciences Meeting & Exhibit, Aerospace Sciences Meetings. American Institute of Aeronautics and Astronautics*, 2002.
 - [22] H.D. Taylor. Increasing the efficiency of the U.A.C. 8-ft wind tunnel fan by means of vortex generators. Technical Report R-4012-4, U.A.C, 1947.
 - [23] N. Troldborg, N.N Sørensen, P-E Réthoré, and P. van der Laan. A consistent method for finite volume discretization of body forces on collocated grids applied to flow through an actuator disk. *Computers and Fluids*, 2015.
 - [24] N. Troldborg, F. Zahle, and N.N Sørensen. Simulation of a MW rotor equipped with vortex generators using CFD and an actuator shape model. *53rd AIAA conference*, 2015.
 - [25] C.M. Velte. *Characterization of Vortex Generator Induced Flow*. PhD thesis, Technical University of Denmark, 2009.